CrossMark

TECHNICAL PAPER

Effect of piezoresistor configuration on output characteristics of piezoresistive pressure sensor: an experimental study

S. Santosh Kumar · B. D. Pant

Abstract Piezoresistive sensing is one of the most frequently used transduction mechanism in pressure sensors. The piezoresistor placement on the diaphragm and the piezoresistor configuration play a pivotal role in determining the output characteristics of a pressure sensor. In this work, two different pressure sensors with different transverse piezoresistor configurations are studied to determine the effect of piezoresistor configuration on the sensitivity and non-linearity of the pressure sensors. A sensor structure with a square diaphragm size of 1,480 μm edge length and diaphragm thickness of 50 μm is chosen for the study. The design considerations for piezoresistor placement and the piezoresistor shapes are discussed in detail. The sensors are fabricated with bulk micromachined diaphragm and polysilicon piezoresistors. The sensor characteristics are determined for three temperatures, namely, −5, 25 and 55 °C and for a pressure range of 0–30 Bar. The characterization results indicate that the design with two piezoresistor arms in transverse piezoresistor configuration (2 × 2 Design) has higher sensitivity than the single arm configuration (2 × 1 Design) by about 25 % at 25 °C but it also has a higher non-linearity. The study shows the importance of selecting the proper piezoresistor configuration in the design of pressure sensors.

S. S. Kumar (✉) · B. D. Pant
CSIR - Central Electronics Engineering
Research Institute (CEERI), Pilani, Rajasthan, India
e-mail: santoshkumar.ceeri@gmail.com

S. S. Kumar · B. D. Pant
Academy of Scientific and Innovative Research (AcSIR),
New Delhi, India

1 Introduction

Piezoresistive and capacitive sensing are two of the most frequently used transduction mechanisms in MEMS sensors used to convert a pressure input into an electrical output (Eaton and Smith 1997). Piezoresistive pressure sensors offer several advantages over capacitive ones owing to advantages such as DC input, high yield and simple signal conditioning circuitry (Kumar and Pant 2014a). Piezoresistive sensors operate based on the property of doped semiconductors wherein they undergo a change in their resistivity when they are stressed. This phenomenon was first reported by Smith (1954). In order to achieve the purpose of detecting the pressure input, a resistor is subjected to stress using a pressure load by placing it on a diaphragm. Although a single resistor can also perform the function of determining the pressure input based on change in resistance (Chung et al. 1991; Motorola 1998), usually, four piezoresistors (connected in Wheatstone bridge configuration) are used for this purpose. Using a Wheatstone bridge helps in cancelling out the temperature effects due to TCR (Kumar and Pant 2014b). Different materials have been reported to exhibit the property of piezoresistance, such as silicon (Zhang et al. 2007; Bian et al. 2009), polysilicon (Tsai et al. 2009; Malhaire and Barbier 2003), silicon carbide (Fraga et al. 2010; Wu et al. 2006), carbon fibre (Park et al. 2007), diamond (Werner et al. 1998; Wur et al. 1995) etc. Generally, silicon or polysilicon based piezoresistors are used in pressure sensor because of well-established fabrication processes for realizing the sensors. Silicon piezoresistors show a better sensitivity compared to polysilicon based piezoresistors (Peng et al. 2005). However, silicon piezoresistors are isolated by a p-n junction from the bulk and thus cannot be used above 125 °C due to

high leakage current (Guo et al. 2009). Polysilicon based pressure sensors can work at high temperature because the piezoresistors are isolated from each other and from the bulk using an isolating oxide layer (Kumar et al. 2014). Silicon-on-insulator (SOI) based pressure sensors also can achieve the purpose of high temperature operation due to the presence of buried oxide layer but they are not as economical as polysilicon based sensors due to high cost of starting substrate.

The schematic of a piezoresistive pressure sensor is shown in Fig. 1. The diaphragm of the sensor can be formed using wet bulk micromachining with alkali hydroxides such as potassium hydroxide (KOH) and tetramethylammonium hydroxide (TMAH) (Tokoro et al. 1998; Kumar and Pant 2013; Mukhiya et al. 2006). The piezoresistors are placed at high stress regions close to the diaphragm edges for experiencing maximum stress and they are connected in Wheatstone bridge as shown in Fig. 1a. Transverse piezoresistor (R_1 and R_4) have their longer edges parallel to the diaphragm edge and undergo a decrease in resistance due to transverse stress. Longitudinal piezoresistor (R_2 and R_3) have their longer edges perpendicular to the diaphragm edge and undergo an increase in resistance due to longitudinal stress. The output voltage of the sensor under a pressure load is given by (Senturia 2001):

$$V_{out} = V_+ - V_- = \left(\frac{\alpha_1 + \alpha_2}{2(1 + \alpha_1 - \alpha_2)} \right) V_{in} \qquad (1)$$

where α_1 and $-\alpha_2$ are the relative change in resistances of longitudinal and transverse piezoresistors, respectively. V_{in} is the input voltage bias to the Wheatstone bridge.

The design optimization of pressure sensors involves optimizing the diaphragm size, diaphragm thickness and the piezoresistor placement at high stress regions. The shape and configuration of piezoresistors can also play an important role in determining the output characteristics of the sensor. Pressure sensors with different piezoresistor configurations in terms of size and number of piezoresistor turns have been reported in literature (Clark and Wise 1979; Malhaire and Barbier 2003; Zhang et al. 2007). The analytical tools proposed for calculating the sensitivity and non-linearity of pressure sensors either consider point resistors or rectangular resistors and therefore have limited application (Maier-Schneider et al. 1995; Gong and Lee 2001). Therefore, it is often beneficial to carry out an experimental study for determining the effect of piezoresistor configuration on sensor characteristics. The experimental study of the effect of different piezoresistor configuration for silicon piezoresistors has been carried out (Zhang et al. 2007) but no such comparative study has been carried out for the polysilicon piezoresistors to the best of our knowledge. In this work, a comparative study of two different types of piezoresistor configurations is carried out and their effect on the output characteristics of the sensor is determined. The paper starts with the design considerations and finite element method (FEM) analysis of the diaphragm structure to determine the piezoresistor placement. Next, the piezoresistor configurations

Fig. 1 Schematic view of a piezoresistive pressure sensor. **a** Piezoresistor placement and connections. **b** Slanted wall cavity formed using wet bulk micromachining
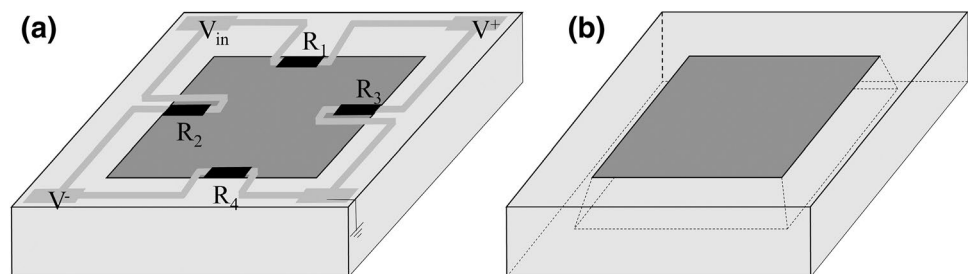

Fig. 2 Contour plot of results obtained using FEM design simulations. **a** Diaphragm deflection. **b** von-Mises stress distribution
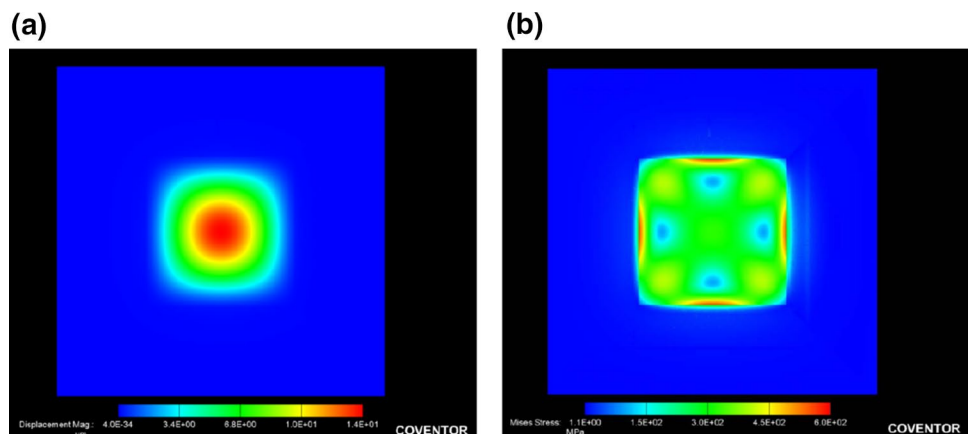
(a)

(b)

Cutline-2

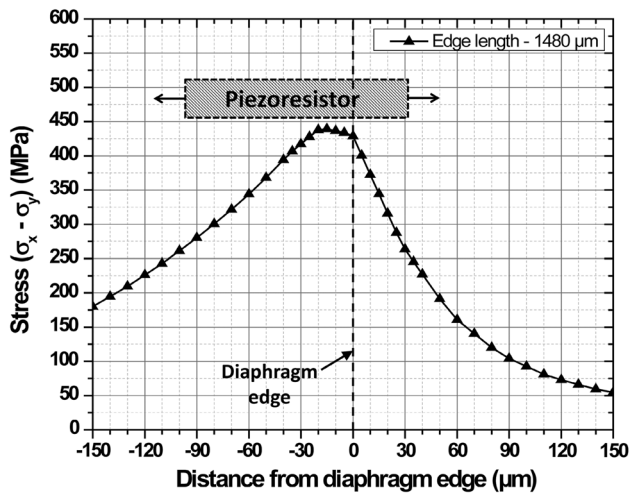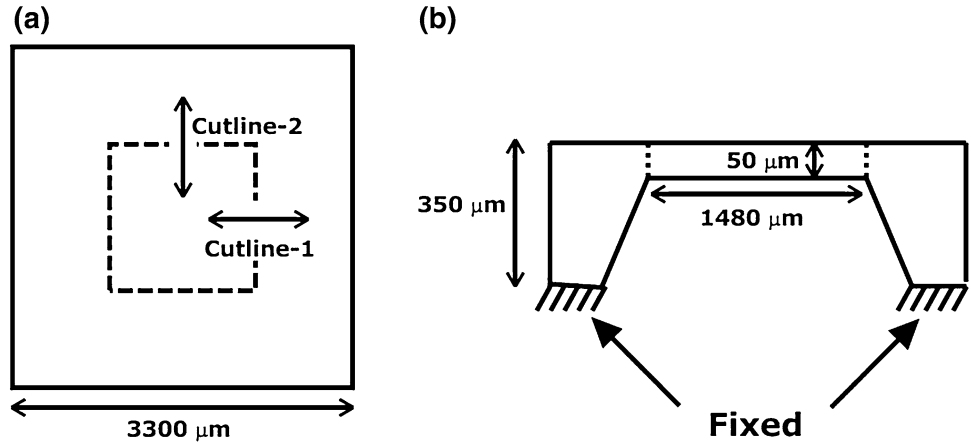Cutline-1

3300 µm

50 µm

1480 µm

350 µm

Fixed

Fig. 4 Differential stress along Cutline-1 for longitudinal piezoresistor placement optimization
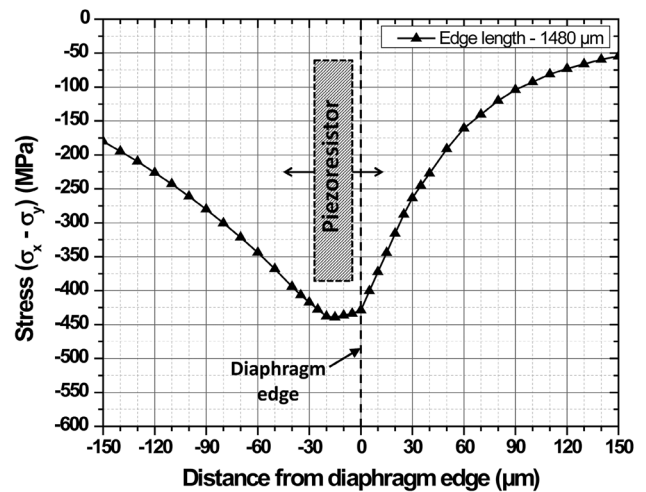

Fig. 5 Differential stress along Cutline-2 for transverse piezoresistor placement optimization

are explained. Finally, the device fabrication, characterization setup and the testing results are reported.

2 Design consideration and piezoresistor configurations

There are various parameters of output characteristics for a piezoresistive pressure sensor such as sensitivity, non-linearity, hysteresis, temperature drift etc. However, the first two, namely, sensitivity and non-linearity are important at the design stage. A typical diaphragm size of 1,480 µm × 1,480 µm and a diaphragm thickness of 50 µm are chosen for the study. As the purpose of this study is not optimization of output characteristics but the study of effect of piezoresistor configuration, therefore, a slightly larger diaphragm size is chosen to obtain good sensitivity in the pressure range of 0–30 Bar. This higher sensitivity comes at the cost of reduced linearity but will help in giving a clearer picture of the effect of the two different piezoresistor

configurations on the sensitivity and non-linearity. The contour plot for diaphragm deflection and von-Mises stress distribution of the sensor structure at full scale pressure (30 Bar) obtained by FEM simulations using CAD tool Coventorware® are depicted in Fig. 2. The plots show that the maximum deflection of the diaphragm is at the center of the diaphragm and the maximum von-Mises stress is concentrated close to the four edges of the diaphragm. Thus, the piezoresistors are placed close to the diaphragm edges.

The output (and therefore the sensitivity) of the pressure sensor is proportional to the differential stress at the piezoresistor location and can be expressed by the approximate expression (Li et al. 2012):

$$V_{out} = \frac{V}{2}\pi_{44}(\sigma_x - \sigma_y) \tag{2}$$

where, $\sigma_x - \sigma_y$ is the differential stress at the piezoresistor locations and π_{44} is the shear piezoresistive coefficient.
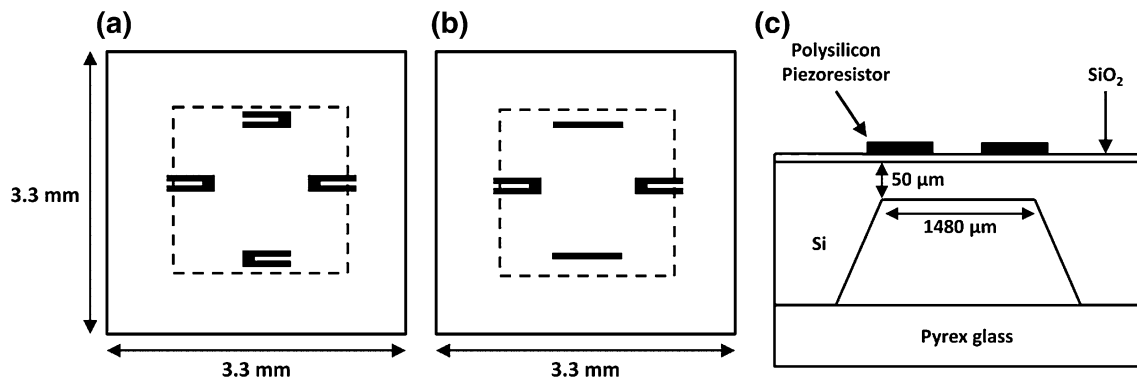
Fig. 6 **a** Top view of sensor structure for 2 × 2 Design. **b** Top view of sensor structure for 2 × 1 Design. **c** Cross-sectional view of sensor structure with piezoresistors

Fig. 7 Shape and positioning of transverse piezoresistor in 2 × 1 Design
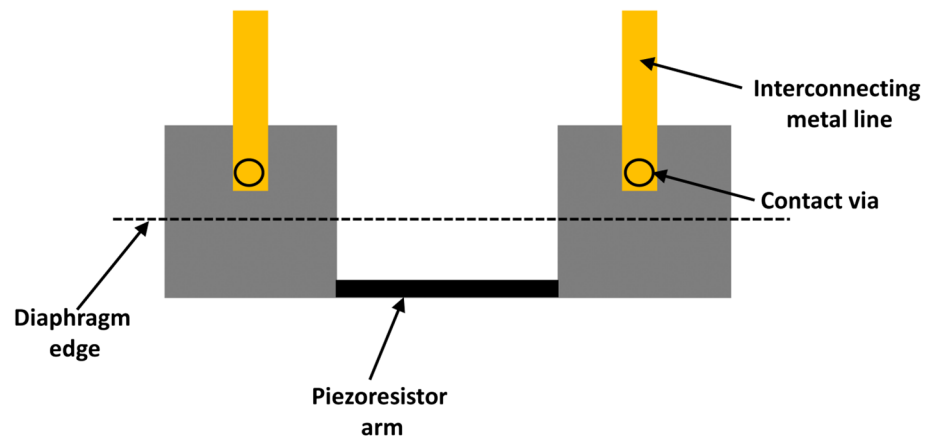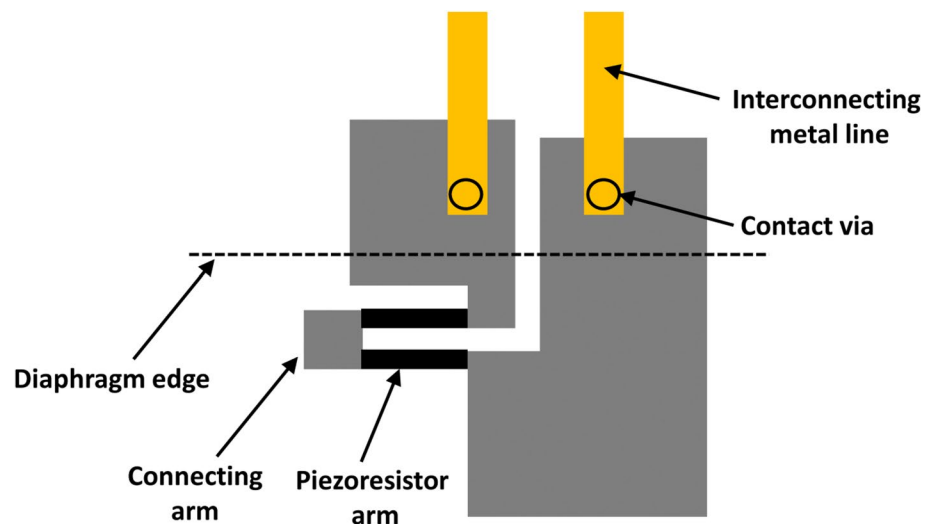

Fig. 8 Shape and positioning of transverse piezoresistor in 2 × 2 Design

Thus, the differential stress on piezoresistors is an important indicator of the output voltage of the sensor. Using the FEM simulation results, the differential stress along two cutlines as shown in Fig. 3a are determined. The two cutlines are near the diaphragm edge and extend 150 μm inside and outside the diaphragm edge. The shape and dimension
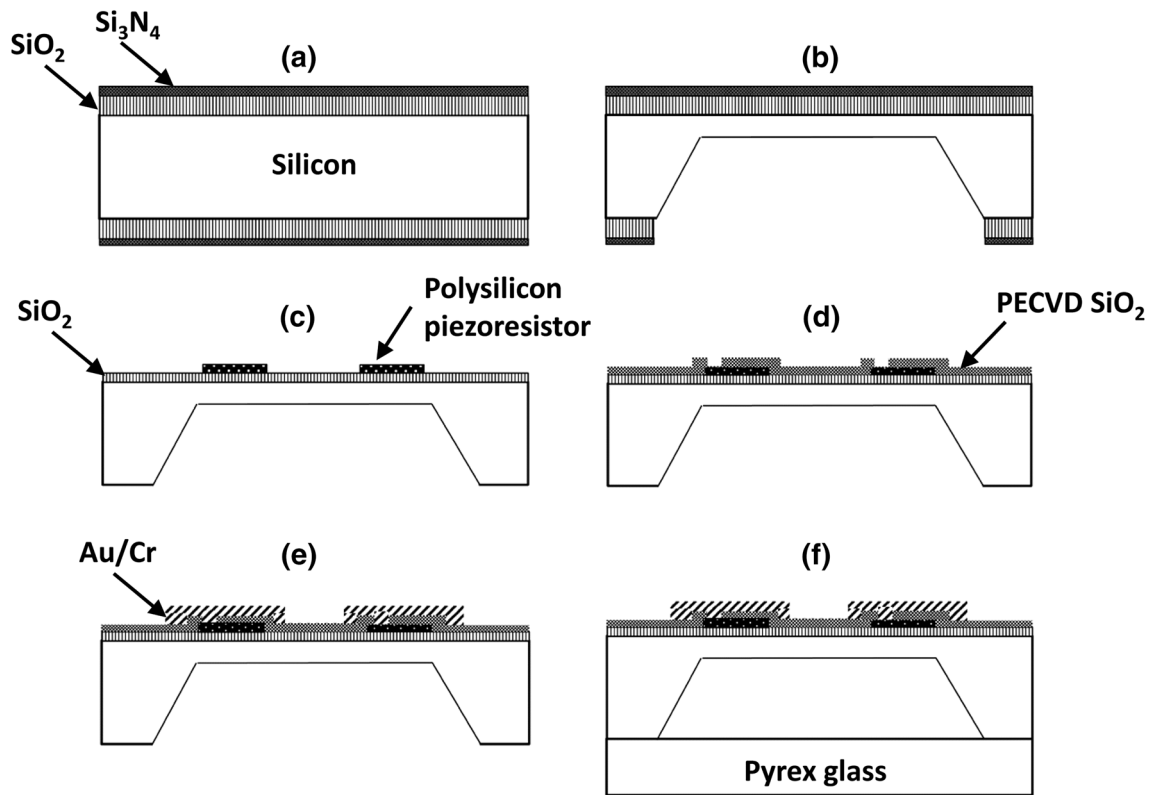
Fig. 9 Fabrication process sequence. **a** Thermal oxide growth and LPCVD silicon nitride deposition. **b** Wet bulk micromachining using TMAH. **c** LPCVD polysilicon deposition, doping and piezoresistor pattering. **d** PECVD oxide deposition and contact via opening. **e** Au/Cr sputtering and patterning. **f** Anodic bonding with Pyrex glass
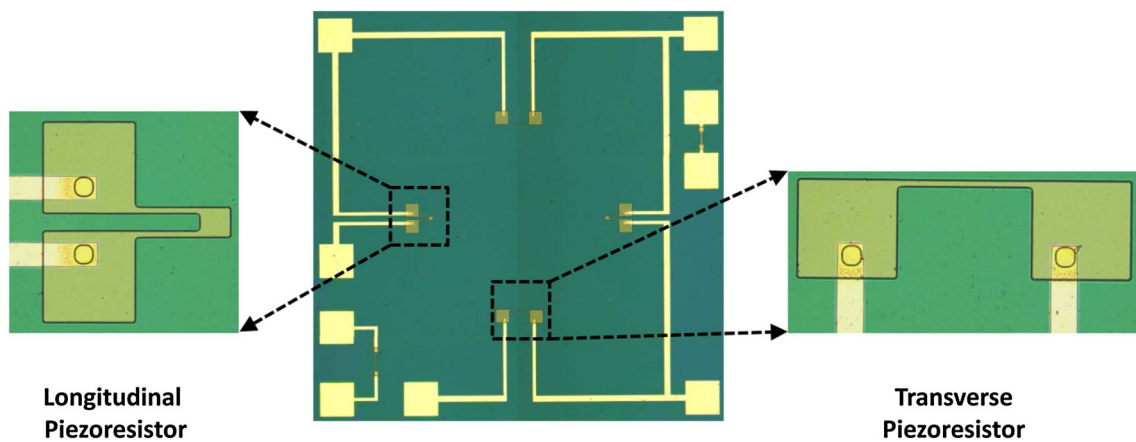

Fig. 10 Microphotograph of fabricated device (2 × 1 Design) with insets showing longitudinal and transverse piezoresistor shapes

of sensor structure used for simulation is shown in Fig. 3b. The structure is clamped from the bottom as shown in the figure to accurately simulate the real clamping conditions. The differential stress along Cutline-1 and Cutline-2 will help determine the position of longitudinal and transverse piezoresistors, respectively.

The plot of differential stress along Cutline-1 is shown in Fig. 4. The values of the differential stresses are positive indicating that the longitudinal piezoresistors will undergo an increase in resistance when the diaphragm is under stress due to a pressure load. The longitudinal piezoresistors are placed lengthwise along Cutline-1 where
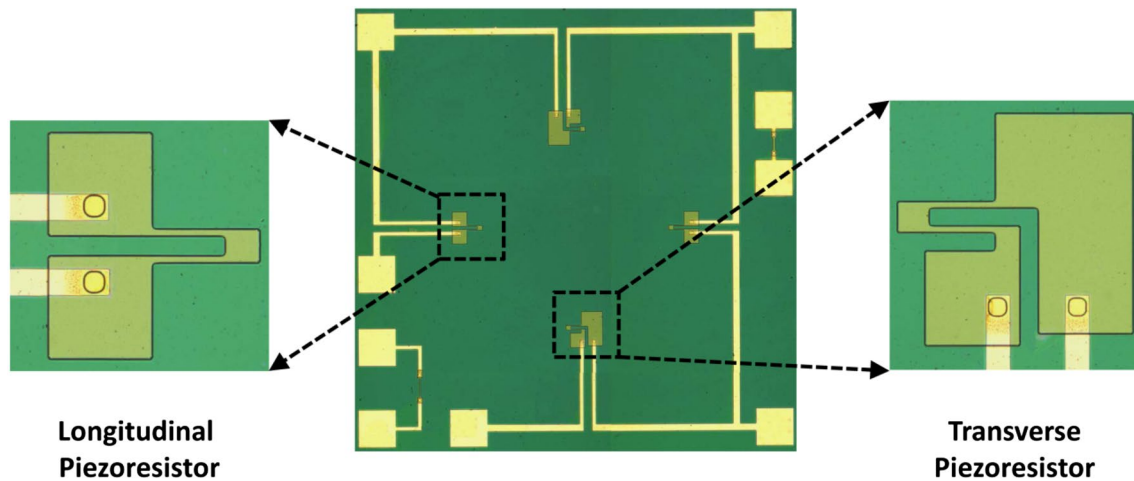
Fig. 11 Microphotograph of fabricated device (2 × 2 Design) with insets showing longitudinal and transverse piezoresistor shapes
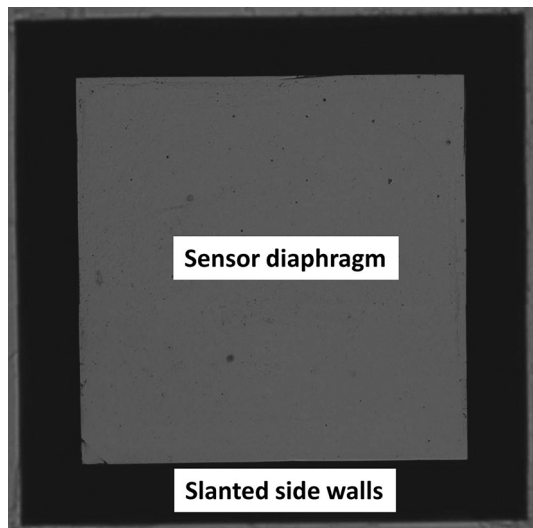

Fig. 12 Microphotograph of *back side* of sensor showing cavity etched using bulk micromachining

the differential stress is maximized. Similarly, the plot of differential stress along Cutline-2 is shown in Fig. 5. The values of the differential stresses are negative indicating that the transverse piezoresistors will undergo a decrease in resistance when the diaphragm is under stress due to a pressure load. The transverse piezoresistors are placed breadthwise along Cutline-2 at a position where the differential stress is minimized. Using the above methodology for determining the piezoresistor locations leads to maximization of the piezoresistor sensitivity.

As can be inferred from Fig. 2b, the high stress regions are long and narrow. Therefore, it is advantageous to have meander-shaped piezoresistors for the longitudinal
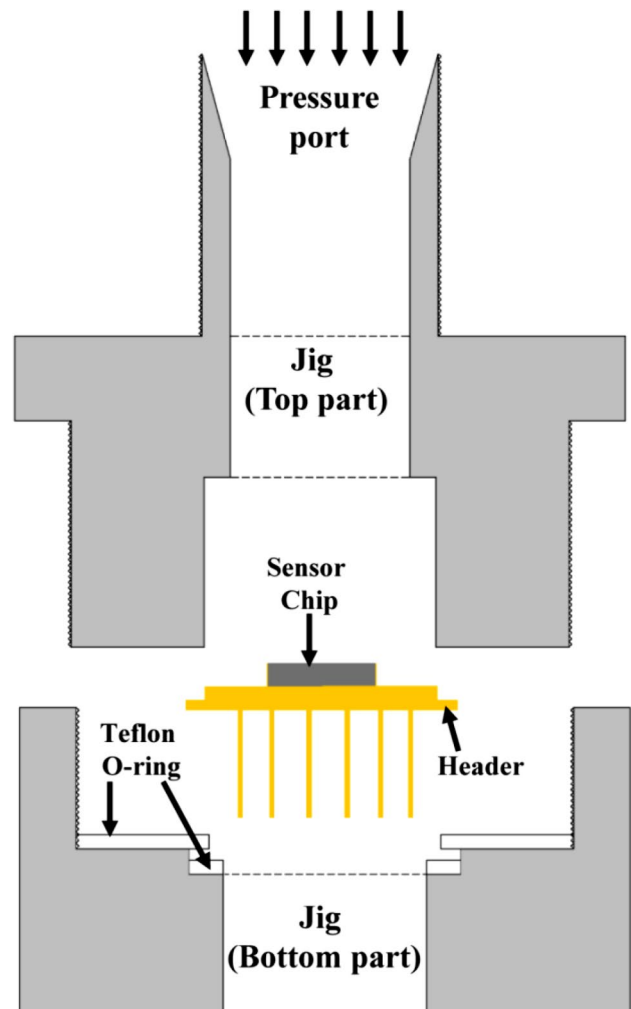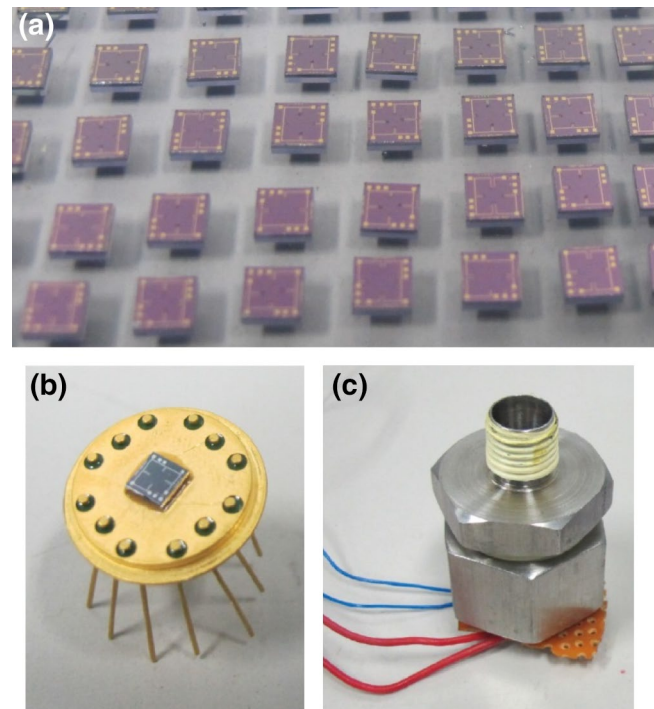

Fig. 13 Cross-sectional view of schematic drawing of pressure sensor jig used for packaging the sensor for pressure testing

piezoresistors to bring the complete piezoresistor inside the high stress region to enhance sensitivity and linearity (Kumar and Pant 2012). However, for the transverse piezoresistors, the piezoresistor shape can either be straight or meander shaped as the long high stress regions lay length wise along the piezoresistor. Keeping in mind the above considerations, two different piezoresistor configurations of transverse piezoresistors and consequently, two different pressure sensor designs are proposed as shown in Fig. 6a, b. The effect of piezoresistors configuration has been explored in an earlier work (Kumar et al. 2013). The design in Fig. 6a is referred to as the '2 × 2 Design' with two piezoresistor arm for both longitudinal and transverse piezoresistors, whereas the design in Fig. 6b is referred to as the '2 × 1 Design' as it has two piezoresistor arm for longitudinal and has single arm for transverse piezoresistors. The cross-sectional schematic view of pressure sensor structure showing the polysilicon piezoresistor and insulating oxide underneath it is shown in Fig. 6c.

While fabricating the devices, the piezoresistors are connected with each other using metal lines. As the diaphragm undergoes deflection with pressure load, it is beneficial to have the metal lines outside the diaphragm edge for reliability. This avoids the mechanical influence of the metal lines on the diaphragm and the influence of the diaphragm deformation on the metal lines (which may lead to their breakage) (Malhaire and Barbier 2003). Repeated stresses during usage can also affect the metal-piezoresistor contact. For this purpose, novel shaped piezoresistors are used for the single arm and double arm transverse piezoresistors.

The transverse piezoresistor shape used for 2 × 1 Design is shown in Fig. 7 and the one used for 2 × 2 Design is shown in Fig. 8.

3 Device fabrication

The device fabrication starts with the growth of 0.6 μm thermal oxide on a 3 inch n-type double side polished (100) silicon substrate. A 0.1 μm LPCVD silicon nitride is then deposited on the wafer as shown in Fig. 9a. After lithography, these two layers are etched using RIE (CF_4 and O_2 chemistry) to form the openings before the next step. These two layers are used for masking during wet bulk micromachining of the silicon wafer using 25 wt.% TMAH to get a diaphragm with 50 μm thickness as shown in Fig. 9b. The silicon etching using TMAH is carried out at 88 °C with an etch rate of about 39 μm/h in the <100> direction. The masking layers are stripped in HF and a fresh thermal oxide with 0.1 μm thickness is grown to perform the function of isolating the piezoresistors from the bulk. Next, a 0.5 μm thick layer of LPCVD polysilicon is deposited on the wafer at 620 °C. The front side of the wafer is implanted with boron ions (dose − 1.5×10^{15} atoms/cm^2, energy − 80 keV) for doping the polysilicon. The wafer is annealed in nitrogen ambient at 1,000 °C for 30 min to activate the dopants. A sheet resistivity of 410–450 Ω/Sq. is obtained. After lithography, the polysilicon layer is etched at selected regions to form the piezoresistor patterns and the oxide and nitride on the back side of the wafer are etched out. This
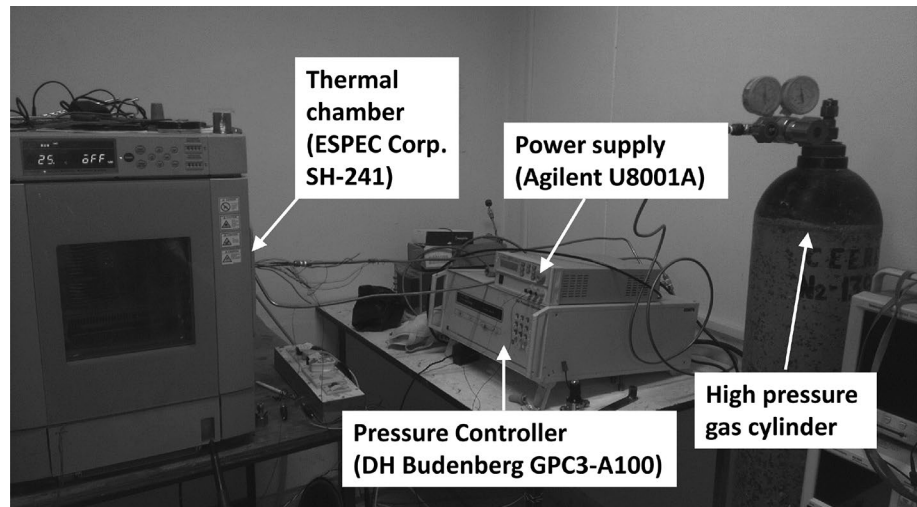
stage is depicted by Fig. 9c. Next, PECVD oxide is deposited on the top side of the wafer at 350 °C (RF power − 80 W) to get an oxide layer of 0.5 μm thickness. Contact vias are opened on this oxide layer using a lithography step as shown in Fig. 9d. Subsequently, Au/Cr (2000 Å/200 Å) is deposited using DC sputtering at a pressure of 5 mTorr and patterned to obtain the Wheatstone bridge connection between the piezoresistors and the contact pads (Fig. 9e). Finally, the wafer is bonded with a Pyrex glass wafer using anodic bonding in vacuum (10^{-6} Bar) as shown in Fig. 9f. This gives a vacuum reference to the pressure sensor (absolute pressure sensor). The resistances of the piezoresistors are in the range of 10–12 kΩ. The microphotograph of the 2 × 1 Design sensor and the 2 × 2 Design sensor are shown in Figs. 10 and 11, respectively. Both the figures have insets depicting the close up view of longitudinal and transverse piezoresistors showing the resistor shapes. Figure 12 depicts the bottom view of the sensor showing the diaphragm cavity.

4 Packaging and characterization setup

After the fabrication of the sensors, the wafer is diced to obtain the individual chips. Both the types of sensors (2 × 1 Design and 2 × 2 Design) are fabricated by putting the design on the same mask set. For obtaining the sensor characteristics, the sensor is first mounted on a header using epoxy and the metal pads on the sensor are wire bonded with the header pins. The header is than placed inside a custom designed jig with a pressure port. The jig consists of two parts. The top part has the pressure port for applying different pressures on the sensor while the bottom part has a hole through which the header pins are available to the outside world for electrical connections. Using
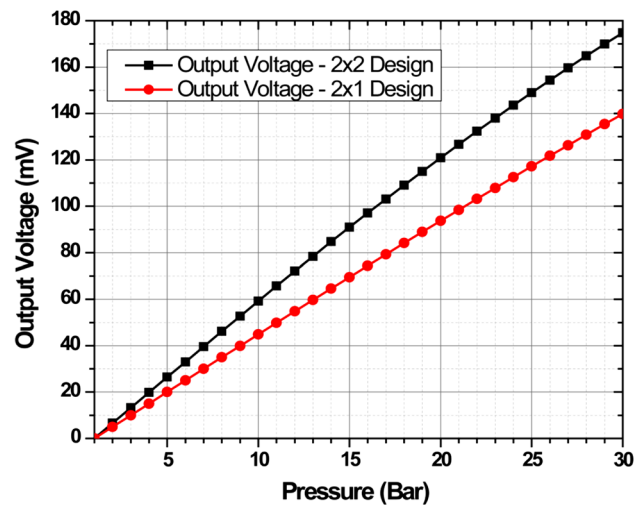

Fig. 16 Sensitivity plot of pressure sensors with different piezoresistor configurations

these electrical connections, the input bias is applied to the Wheatstone bridge and the sensor output is measured. The exploded view of schematic of the jig and the header arrangement is shown in Fig. 13. The header is secured in between the two jigs using two Teflon O-rings to obtain a leak proof arrangement.

The fabricated pressure sensors, a device wire bonded on the header and a jig with ¼ inch pressure port and electrical connections coming out from the back side are shown in Fig. 14a–c, respectively. After packaging the sensor inside the jig, it is placed insde a thermal chamber. Wires for electrical connections are drawn outside and a 3.3 V DC bias is provided to the sensor Wheatstone bridge using an Agilent U8001A power supply. The output of the sensor is measured using a Agilent U1252B digital multimeter. The jig inside the thermal chamber
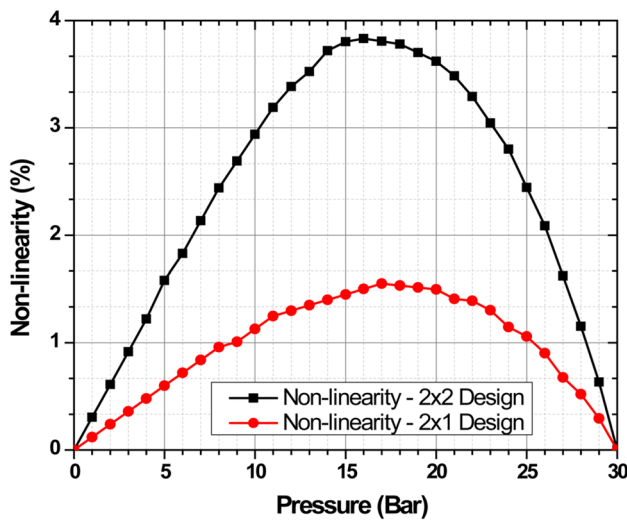
Fig. 17 Non-linearity plot of pressure sensors with different piezoresistor configurations

Table 1 Summary of sensitivity and non-linearity of pressure sensors at different temperatures

Temperature (°C)	Sensitivity (mV/Bar)		Non-linearity (%/Full scale)	
	2 × 1 Design	2 × 2 Design	2 × 1 Design	2 × 2 Design
−5	5.08	6.38	1.65	3.89
25	4.82	6.03	1.55	3.83
55	4.59	5.75	1.52	3.56

is connected to a pressure controller (DH Budenberg GPC3-A100) which in turn is connected with a high pressure gas cylinder. Controlled pressure is applied to the jig (or the sensor) in steps to obtain the output characteristics. Due to unavailability of a vacuum pump, the pressure controller cannot be used to apply a pressure close to vacuum and therefore pressures from 1 to 30 Bars are applied in steps of 1 Bar. The sensor is tested at three temperatures (−5, 25 and 55 °C) (Fig. 15).

5 Characterization results

The sensitivity plot of the two pressure sensors with different piezoresistor configuration is shown in Fig. 16. Both the sensors have non-zero values of output voltage at 1 Bar pressure (minimum pressure applied to the sensor). For the sake of comparison of the output curves of the two sensors, the plot is adjusted for both the curves to have 0 output voltage at 1 Bar pressure. The plot shown in Fig. 16 is for a temperature of 25 °C and similar plots are obtained for −5 and 55 °C. It is clear from the figure that the sensitivity of the 2 × 2 Design is higher than that for 2 × 1 Design, indicating that by using two piezoresistor arms in transverse piezoresistors, the piezoresistors come into high stress regions, thereby increasing the sensitivity. The output voltage of the sensors at vacuum (0 Bar pressure) is calculated by extrapolating the curves. Further, using the end point straight line method (Bao 2005), the sensitivity and non-linearity of each of the sensor at different temperatures is calculated. The non-linearity plot of the two sensors at 25 °C is shown in Fig. 17. The plot indicates that the 2 × 1 Design has a lower non-linearity than the 2 × 2 Design. The summary and comparison of the sensitivity and non-linearity of the sensors at different temperatures is listed in Table 1. The hysteresis for both the sensors at all the temperatures is found to be <0.1 (%/Full scale). Due to the difference in the shape of transverse and longitudinal piezoresistors and different designs of piezoresistors in both the sensors, there is high offset voltage associated with the sensors. The offset voltage of the sensors also drifts with temperature due to temperature coefficient of piezoresistance factor. The offset voltage of the two sensors at different temperatures and the linear fit function for the output of the sensor at different temperatures is listed in Table 2.

6 Conclusions and discussions

In this work, the design considerations, fabrication and static characterization of two sensors is reported. The shape and placement of piezoresistors play an important part in

Table 2 Offset voltage and linear fit function of pressure sensors at different temperatures

Sensor	Temperature (°C)	Offset voltage at 1 Bar (mV)	Linear fit function y = Output voltage (mV) x = Pressure (Bar)
2 × 1 Design	−5	106.6	$y = 5.09x − 102.76$
	25	106.4	$y = 4.84x − 102.61$
	55	106.1	$y = 4.61x − 102.58$
2 × 2 Design	−5	−99.4	$y = 6.43x − 102.13$
	25	−99.2	$y = 6.07x − 101.79$
	55	−99.0	$y = 5.79x − 101.74$

the optimization of a pressure sensor. The aim of the study was to determine the effect of the difference in the transverse piezoresistor configuration on the output characteristics in the two sensors. In the design with two piezoresistor arms in transverse piezoresistor configuration (2×2 Design), the sensitivity is higher than the single arm configuration (2×1 Design) by about 25 % at 25 °C. However the increased sensitivity comes at the cost of greater non-linearity which increases by more than two times its value for 2×1 Design. The output characteristics of the two sensors are determined at three temperatures and the characteristics show similar trends at each temperature. The sensors can be used for applications such dive computers, level indicators, leak detection and industrial control after non-linearity and temperature compensation using appropriate circuitry. Also, the non-linearity of the sensors can be reduced/compensated without compromising on the sensitivity using "stress concentration regions" by structuring the top side of the diaphragm (Bian et al. 2012; Yu et al. 2013; Huang and Zhang 2014). The study shows that the piezoresistor placement and configurations must be carefully chosen for a particular diaphragm size, shape and thickness. The above results may not be applicable for other diaphragm sizes and thicknesses and a similar optimization through experimental methods need to be carried out to determine the most suitable design.

References

Bao M (2005) Analysis and design principles of MEMS devices. Elsevier, Amsterdam

Bian T, Yulong Z, Jiang Z, Zhang L, Liao N, Lio Y, Meng C (2009) The analysis and structural design of micro SOI pressure sensors. In: Proceedings of the 4th international conference on nano/micro eng. and molecular systems, Shenzhen, pp 55–58

Bian T, Yulong Z, Zhuangde J, Bin H (2012) The design and analysis of beam-membrane structure sensors for micro-pressure measurement. Rev Sci Instrum 83:045003

Chung GS, Kawahito S, Ishida M, Nakamura T, Kawashima M, Suzaki T (1991) High-performance pressure sensors using double silicon-on-insulator structures. Rev Sci Instrum 62(5):1341–1346

Clark SK, Wise KD (1979) Pressure sensitivity in anisotropically etched thin-diaphragm pressure sensors. IEEE Trans Electron Devices 26(12):1887–1896

Eaton WP, Smith JH (1997) Micromachined pressure sensors: review and recent developments. Smart Mat Struc 6(5):530–539

Fraga MA, Furlan H, Massi M, Oliveira IC, Koberstein LL (2010) Fabrication and characterization of a SiC/SiO₂/Si piezoresistive pressure sensor. Procedia Eng 5:609–612

Gong SC, Lee C (2001) Analytical solutions of sensitivity for pressure microsensors. IEEE Sens J 1(4):340–344

Guo S, Eriksen H, Childress K, Fink A, Hoffman M (2009) High temperature smart-cut SOI pressure sensor. Sens Actuators A 154:255–260

Huang X, Zhang D (2014) A high sensitivity and high linearity pressure sensor based on a peninsula-structured diaphragm for low-pressure ranges. Sens Actuator A 216:176–189

Kumar SS, Pant BD (2012) Design of piezoresistive MEMS absolute pressure sensor. In: Proceedings of the SPIE 8549

Kumar SS, Pant BD (2013) Effect of temperature on etch rate and undercutting of (100) silicon using 25 % TMAH. In: Proceedings of the international conference on emerging technologies micro to nano (ETMN), Goa

Kumar SS, Pant BD (2014a) Design principles and considerations for the 'ideal' silicon piezoresistive pressure sensor: a focused review. Microsyst Technol 20:1213–1247

Kumar SS, Pant BD (2014b) Polysilicon thin film piezoresistive pressure microsensor: design, fabrication and characterization. Microsyst Technol. doi:10.1007/s00542-014-2318-1

Kumar SS, Ojha AK, Nambisan R, Sharma AK, Pant BD (2013) Design and simulation of MEMS silicon piezoresistive pressure sensor for barometric applications. In: Proceedings of the ARTCom&ARTEE PEIE&itSIP and PCIE. Elsevier, ISBN978-81-910691-8-3, pp 339–345

Kumar SS, Ojha AK, Pant BD (2014) Experimental evaluation of sensitivity and non-linearity in polysilicon piezoresistive pressure sensors with different diaphragm sizes. Microsyst Technol. doi:10.1007/s00542-014-2369-3

Li X, Liu Q, Pang S, Xu K, Tang H, Sun C (2012) High-temperature piezoresistive pressure sensor based on implantation of oxygen into silicon wafer. Sens Actuators A 179:277–282

Maier-Schneider D, Maibach J, Obermeier E (1995) A new analytical solution for the load-deflection of square membranes. J Microelectromech Syst 4:238–241

Malhaire C, Barbier D (2003) Design of a polysilicon-on-insulator pressure sensor with original polysilicon layout for harsh environment. Thin Solid Films 427:362–366

Motorola (1998) Sensor Device Data/Handbook 4th edn. Motorola Inc., Phoenix

Mukhiya R, Bagolini A, Margesin B, Zen M, Kal S (2006) (100) Bar corner compensation for CMOS compatible anisotropic TMAH etching. J Micromech Microeng 16:2458–2462

Park CS, Kang BS, Lee DW, Choi TY, Choi YS (2007) Fabrication and characterization of a pressure sensor using a pitch-based carbon fibre. Microelectron Eng 84:1316–1319

Peng CT, Lin JC, Lin CT, Chiang KN (2005) Performance and package effect of a novel piezoresistive pressure sensor fabricated by front-side etching technology. Sens Actuators A 119(1):28–37

Senturia SD (2001) Microsystem design. Kluwer, Boston

Smith CS (1954) Piezoresistance effect in germanium and silicon. Phys Rev 94:42–49

Tokoro K, Uchikawa D, Shikida M, Sato K (1998) Anisotropic etching properties of Silicon in KOH and TMAH solutions. In: Proceedings of the international symposium on micromechatronics and human science, pp 65–70

Tsai HH, Hsieh CC, Fan CW, Chen YC, Wu WT (2009) Design and characterization of temperature-robust piezoresistive micropressure sensor with double-wheatstone-bridge structure. In: Proceedings of the symposium on design, test, integration and packaging of MEMS/MOEMS, Rome, pp 363–368

Werner M, Gluche P, Adamschik M, Kohn E, Fecht HJ (1998) Review on diamond based piezoresistive sensors. Proc IEEE Int Symp Ind Electron 1:147–152

Wu CH, Zorman CA, Mehregany M (2006) Fabrication and testing of bulk micromachined silicon carbide piezoresistive pressure sensors for high temperature applications. IEEE Sens J 6:316–324

Wur DR, Davidson JL, Kang WP, Kinser DL (1995) Polycrystalline diamond pressure sensor. J Microelectromech Syst 4(1):34–41

Yu ZL, Zhao YL, Sun L, Tian B, Jiang ZD (2013) Incorporation of beams into bossed diaphragm for a high sensitivity and overload micro pressure sensor. Rev Sci Instrum 84:015004

Zhang YH, Yang C, Zhang ZH, Lin HW, Liu LT, Ren TL (2007) A novel pressure microsensor with 30-µm-thick diaphragm and meander-shaped piezoresistors partially distributed on highstress bulk silicon region. IEEE Sens J 7(12):1742–1748